Journal of Wind Engineering & Industrial Aerodynamics 166 (2017) 106–116

Contents lists available at ScienceDirect

Journal of Wind Engineering and Industrial Aerodynamics

journal homepage: www.elsevier.com/locate/jweia

CFD simulations of wind loads on a container ship: Validation and impact of geometrical simplifications

W.D. Janssen[a,b,*], B. Blocken[b,c], H.J. van Wijhe[a]

[a] Harbor Master's Division, Port of Rotterdam, The Netherlands
[b] Building Physics and services, Department of the Built Environment, Eindhoven University of Technology, The Netherlands
[c] Building Physics section, Department of Civil Engineering, KU Leuven, Belgium

ARTICLE INFO

Keywords:
Ship aerodynamics
Naval wind environment
Computational fluid dynamics (CFD)
Wind tunnel experiments
Force coefficients

ABSTRACT

Due to the increasing windage area of container ships, wind loads are playing a more important role in navigating the ship at open sea and especially through harbor areas. This paper presents 3D steady RANS CFD simulations of wind loads on a container ship, validation with wind-tunnel measurements and an analysis of the impact of geometrical simplifications. For the validation, CFD simulations are performed in a narrow computational domain resembling the cross-section of the wind tunnel. Blockage effects caused by the domain boundaries are studied by comparing CFD results in the wind tunnel domain and a larger domain. The average absolute difference in numerically simulated and measured total wind load on the ship ranges from 37.9% for a simple box-shaped representation of the ship to only 5.9% for the most detailed model. Modeling the spaces in-between containers on the deck shows a 10.4% average decrease in total wind load on the ship. Modeling a more slender ship hull while keeping the projected front and side area of the ship similar, yields an average decrease in total wind load of 5.9%. Blockage correction following the approach of the Engineering Sciences Date Unit underestimates the maximum lateral wind load up to 17.5%.

1. Introduction

Due to the trend of increasing ship sizes, the wind loads on a ship are playing a more important role in navigating the ship under high winds at open sea and especially in the harbor where the ship is being maneuvered in confined spaces. In the harbor, accurate knowledge of the wind loads is also important to determine berth requirements such as safe working loads of bollards and characteristics of fenders. Wind coefficients used in practice for a ship at open sea are often taken from literature, i.e. OCIMF (1994) and SIGTTO (2007), empirical methods (Haddara and Guedes Soares, 1999), or obtained from wind tunnel tests. Many wind tunnel studies are not a public open resource, although exceptions are for instance the wind tunnel database by Blendermann (1996) and a study of wind loads on a 9000+TEU container ship by Andersen (2013). Also numerical simulation by Computational Fluid Dynamics (CFD) can be used for the assessment of the wind loads.

The use of CFD in wind engineering, also referred to as Computational Wind Engineering, has seen a rapid growth in the past 50 years (Murakami, 1997; Stathopoulos, 1997; Baker, 2007; Solari, 2007; Meroney and Derickson, 2014; Blocken, 2014, 2015; Meroney, 2016; Tominaga and Stathopoulos, 2016). Indeed, also concerning wind loads on ships, several CFD studies have been published, several of which include a comparison between CFD simulations and wind tunnel measurements. Wnęk and Guedes Soares (2015) focused on the wind load on an LNG carrier with a very specific geometrical shape. Koop et al. (2012) compared wind tunnel measurements and CFD simulations for five different ship types: (1) a Moss type LNG carrier; (2) a membrane type LNG carrier; (3) a shuttle tanker at 10 m draft; (4) a shuttle tanker at 22 m draft; and (5) an FPSO (Floating, Production, Storage and Offloading vessel). Both Wnęk and Guedes Soares (2015) and Koop et al. (2012) show good results when comparing the force coefficients C_X, C_Y and C_N obtained from CFD simulations with wind tunnel data. However, the results of the comparison were provided in graphical form but not in an overall percentage difference between wind tunnel and CFD data. None of these studies however provided a detailed analysis of the impact of geometrical simplifications on the predicted wind loads.

This paper presents wind load simulations on a container ship at open sea. The Port of Rotterdam is interested in wind force coefficients for a wide range of ships, which can be provided using CFD simulations. However the results of these CFD simulations require solution

* Corresponding author at: Building Physics and services, Department of the Built Environment, Eindhoven University of Technology, The Netherlands.
E-mail addresses: wd.janssen@portofrotterdam.com, w.d.janssen@tue.nl (W.D. Janssen).

http://dx.doi.org/10.1016/j.jweia.2017.03.015
Received 25 January 2017; Received in revised form 21 March 2017; Accepted 27 March 2017

verification and validation. The current study focuses both on the validation and on the impact of geometrical simplifications of the ship's hull and on-deck container stacks on the obtained wind load. The validation is performed by comparison with wind tunnel data of force coefficients from Andersen (2013). The outline of the paper is as follows. First, the definition of forces and coefficients is provided in Section 2. Next, the wind tunnel measurement setup (Section 3) and the CFD simulations (Section 4) are described. Since the blockage ratio of the ship in the wind tunnel is high, measured and simulated force coefficient values are corrected for blockage in Section 5. In Section 6, the corrected force and moment coefficients of the simple to detailed container ship geometries are compared to the measurement results. In addition, the impact of geometrical simplifications on the total ship wind load is discussed. Next, the ship is placed in a larger domain to study the impact of wind flow blockage caused by the domain wall boundaries. These CFD results are also described in this section. The paper concludes with discussion, future work, and conclusions.

2. Definition of loads and coefficients

The coordinate system of the ship is different from the coordinate system of the wind tunnel/CFD domain used in this paper. The ship coordinate system, shown in Fig. 1, has its origin on the ship centreline, halfway the length between perpendiculars ($L_{pp}/2$), here based on the hull at the waterline. The axes are defined as follows:

- The x-axis is positive forward
- The y-axis is positive to starboard
- The z-axis is positive downward.

The forces studied in this paper are shown in Fig. 1, they are:

- The longitudinal force X (N)
- The lateral force Y (N)
- The moment about the z-axis N (Nm); positive when the ship bow moves to starboard.

The longitudinal force X, the lateral force Y, and the moment around the z-axis N are made non-dimensional as follows:

$$C_X = \frac{X}{\frac{1}{2}\cdot\rho\cdot U^2\cdot A_f}$$
$$C_Y = \frac{Y}{\frac{1}{2}\cdot\rho\cdot U^2\cdot A_s}$$
$$C_N = \frac{N}{\frac{1}{2}\cdot\rho\cdot U^2\cdot A_s\cdot L_{oa}} \quad (1)$$

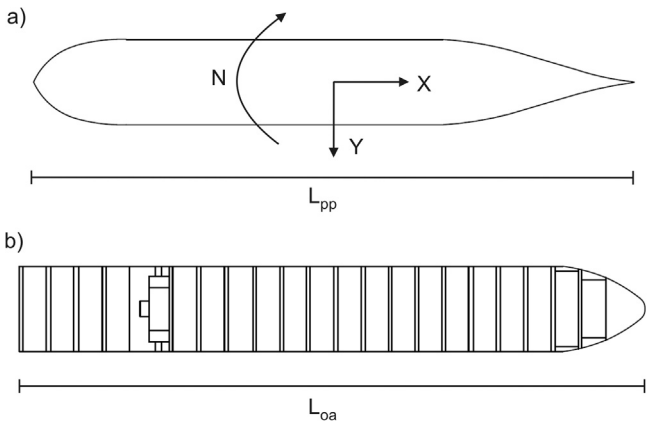

Fig. 1. a) Definition of forces X and Y, and moment N. The origin is located halfway the length between perpendiculars (L_{pp}) here based on the hull at the waterline b) Top view of the ship, showing the length over all (L_{oa}).

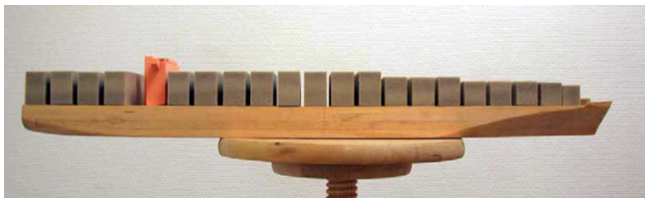

Fig. 2. Wind tunnel model of the container ship (© Elsevier, reproduced with permission; source: Andersen (2013)).

where

ρ=the density of air (=1.225 kg/m^3 at 15 °C).
U=the wind flow velocity experienced by the ship (m/s)
A_f=projected front area of the ship (m^2)
A_s=projected side area of the ship (m^2)
L_{oa}=length over all of the ship (see Fig. 1b)

3. Wind tunnel measurement setup

3.1. Test section and model geometry

A wind tunnel study on wind loads on a post-Panamax container ship was performed by Andersen (2013). A 9000+TEU container ship at scale 1/450 (see Fig. 2) was tested in a closed-loop low-speed boundary layer wind tunnel at FORCE Technology in Kongens, Lyngby, Denmark. The wind tunnel test section has dimensions L×W×H=2.6×1.0×0.7 m^3, with chamfered corners of 0.11 m, as shown in Fig. 3. The container ship was placed in the middle of a turntable with the center point located at 0.79 m from the inlet of the measurement section. For the current study Andersen agreed to share the drawings of the wooden ship model since the CAD drawings are confidential. Roughly the fully loaded ship model size is L×W×H=0.750×0.101×0.077 m^3, where the height originates from the distance between the water line to the top of the highest container stacks (7 high) that cover more than half the ship. The bridge of the ship, depicted in orange in Fig. 2, is located higher, up to about 0.10 m at reduced scale. In full scale this container ship is approximately 340 m long, 45 m wide and 35 m high. The projected front area of the reduced-scale model is A_f=0.0096 m^2 and the projected side area is A_s=0.05 m^2. The length over all L_{oa} is 0.75 m (full scale 340 m) and the length between perpendiculars L_{pp} is 0.71 m (full scale 320 m). In the wind tunnel study by Andersen, more configurations were studied but these are not taken into consideration for the current study since the ship with full load will have the largest wind load. Wind tunnel tests were performed for 19 different wind angles at 10° intervals. The ship is symmetrical with respect to its longitudinal centerline, therefore measurements for the other 17 wind directions were not performed.

3.2. Experimental conditions

Vertical mean wind speed and streamwise turbulence intensity profiles were measured at the center of both turntables in the wind tunnel, located at 0.79 m and 1.94 m downstream from the inlet of the measurement section, with the ship model absent. Note that measuring these profiles at the location of the turntable (=incident profiles) is better than measuring them at the inlet of the test section (=approach-flow profiles), as the incident profiles are those that are representative of the results obtained with the model at that position. Earlier research has shown that approach-flow profiles and incident profiles can differ markedly (Blocken et al., 2008). The fact that vertical profiles measured at different locations in the wind tunnel can differ substantially was also demonstrated by Andersen (2013). Fig. 4a shows the vertical mean wind speed profiles measured at both turntables. Above 0.04 m from the wind tunnel floor, the mean wind velocity is larger when measured

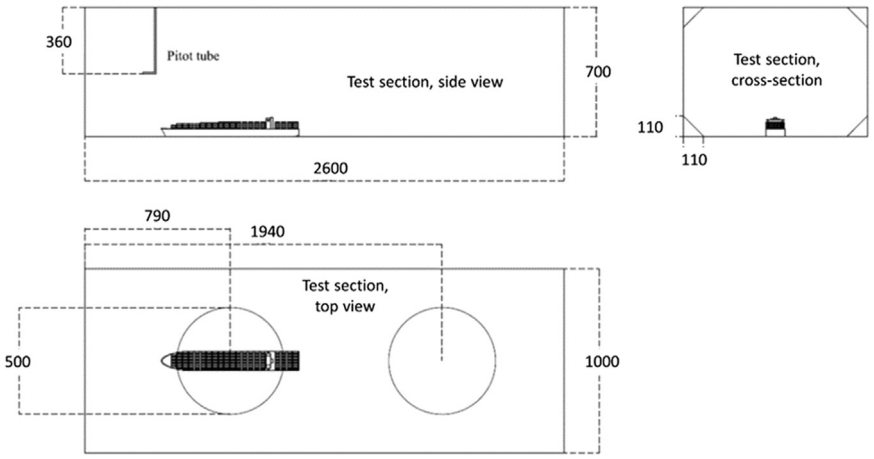

Fig. 3. Wind tunnel test section and position of model on upstream turntable. Dimensions in mm (© Elsevier, reproduced with permission; modified from Andersen (2013)).

more downstream in the empty wind tunnel. Andersen also provided the target wind velocity profile (Fig. 4, solid line), which is a power law with z_{ref}=0.0222 m (equal to 10 m height in full scale), U_{ref}=45 m/s and α=0.11:

$$U(z) = U_{ref}\left(\frac{z}{z_{ref}}\right)^{\alpha} \quad (2)$$

For velocity profiles over the ocean, α is usually between 0.11 and 0.14, which is the target value for wind tunnel tests of ocean structures (Norwegian Maritime Directory, 1997). Fig. 4b shows the measured streamwise turbulence intensity above the turntables. At 0.79 m downstream it ranges from nearly 12% near floor level to less than 1% above z=0.04 m. The actual measurements were performed with the model on the first turntable. Reference wind speed U_{ref}=45 m/s at reference height z_{ref}=0.0222 m (or 10 m at full scale) yields a Reynolds number based on the ship characteristic length L_{pp}=0.71 m of 2.1×10^6. Based on the ship width, the Reynolds number is 0.3×10^6. Because the ship is a bluff body with sharp edges, the separation points will be located at these edges and the flow can be considered similar to that in full scale. The measurement results for the wind loads will be reported together with the CFD results in Section 6.

4. CFD simulation setup

4.1. Computational geometry and grid

The geometry of the computational domain is shown in Fig. 5a, and is similar to the geometry of the wind tunnel, however without the chamfered corners.

Simulations are performed with four configurations of the container ship geometry ranging from a simple rectangular box (configuration A) to a fairly detailed container ship where also the spacing between the containers and the specific shape of the hull is taken into account (configuration D). The ship dimensions and placement in the domain are based on the wind tunnel setup as discussed in Section 3.1. The ship geometries and grids are generated simultaneously with the

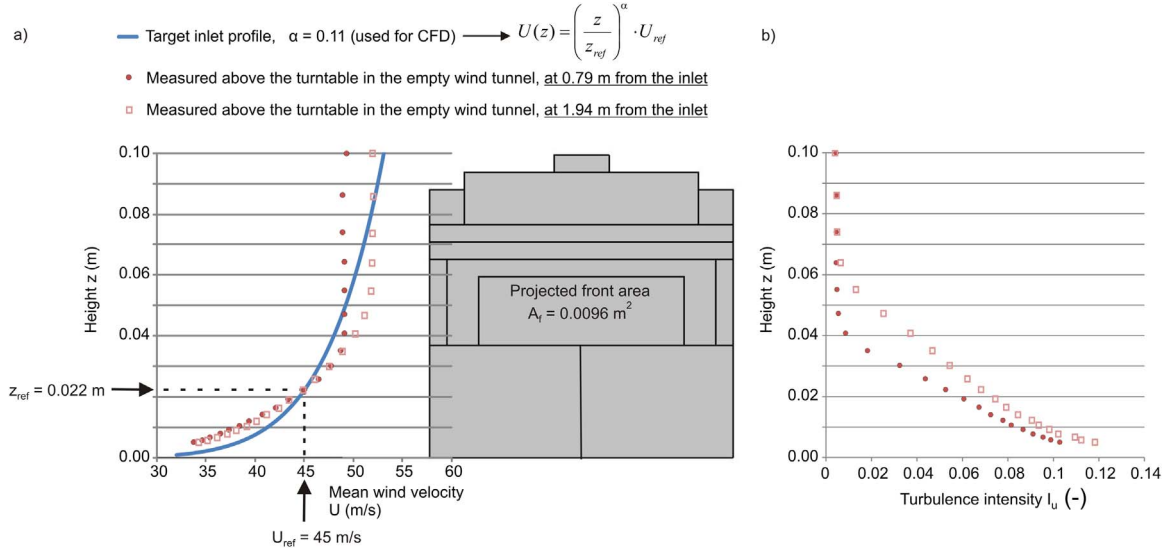

Fig. 4. a) Measured vertical mean wind velocity profiles at the center of the two turntables in the empty wind tunnel at 0.79 m (solid circles) and 1.94 m (open squares) from the inlet. The solid blue line represents the target inlet profile. Note that the mean wind velocity axis starts at 30 m/s and that the ship height in Fig. 4a includes the height of the bridge, yielding an overall height about 0.10 m. b) Measured vertical streamwise turbulence intensity at the center of the two turntables. (For interpretation of the references to color in this figure legend, the reader is referred to the web version of this article.)

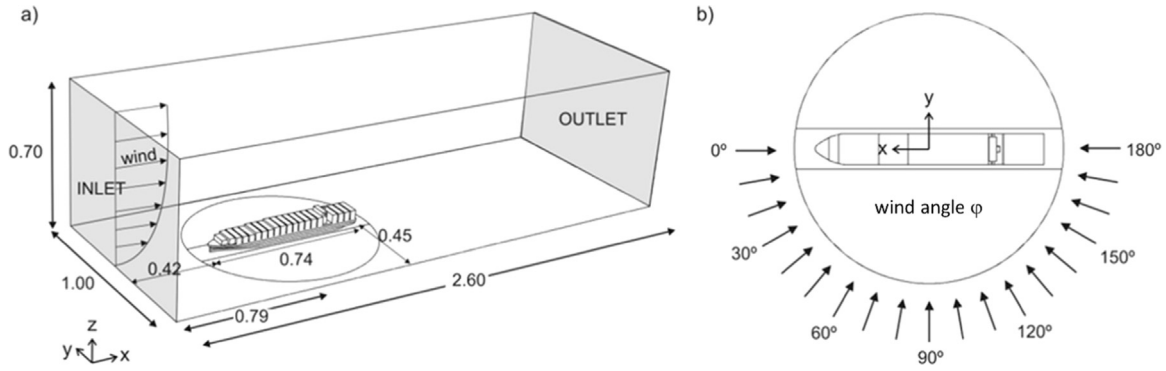

Fig. 5. (a) Computational domain at scale 1/450, showing the inlet and outlet in gray, while the other sides are walls. Dimensions in m. (b) 19 wind angles φ for measurements and simulations.

software Gambit 2.4.6 using the surface-grid extrusion technique by van Hooff and Blocken (2010) which allows creating a high quality grid consisting only of hexahedral cells. Fig. 6 shows these four different geometrical configurations together with the grid on the model surfaces:

– Configuration A is the most basic form, a simple rectangular box. It has dimensions L×W×H=0.740×0.101×0.077 m^3 (333.00×45.45 ×34.65 m^3 at full scale). The computational grid contains 206 cells over the length, 24 cells over the width and 32 cells over the height of the box. For the box geometry the origin of the axes is set at the intersection of halfway the width and halfway the length of the box. The cell resolution footprint on the hull is approximately 0.0036×0.0022 m^2 (1.6×1.0 m^2 in full scale) to ensure a smooth transition to the outer domain, which is equal to the outer domain of configuration C and D. The total number of cells is 2,866,376.
– Configurations B, C, and D with containers stacked 7 high have the same overall dimensions as the box. The length is somewhat shorter than the ship used for measurements. This is caused by modeling only the ship volume and not the bulwark at the bow.
– Configuration B does not contain the in-between the container stacks and has a simplified hull based on the contour of the ship at deck level. The hull contour of the bow is equal at water and deck level and is shifted over a diagonal line using the surface-grid extrusion technique. The cell resolution footprint on the hull is approximately 0.0044×0.0044 m^2 (2×2 m^2 in full scale). The total number of cells is 1,541,840.
– Configuration C has the same hull but the spaces in-between the container stacks are taken into account. The spacing is bridged with four grid cells over a full scale width of 2.5 m. Following international best practice guidelines (Franke et al., 2007; Tominaga et al., 2008) would require at least 10 cells in this void between the container stacks. However, in order to reduce the overall cell count and keep grid stretching ratios within limits, less cells are used here. The cell resolution footprint on the hull is approximately 0.0022×0.0022 m^2 (1×1 m^2 in full scale) to obtain a smooth transition of cells at the hull to those near the container stacks and the gaps. The total number of cells is 3,970,994.
– Finally, configuration D shows a more slender hull of the ship which is based on hull contours at four different heights obtained from drawings of Andersen. However, since the grid extrusion technique is used, the hull consists of several subdomain grids that are not conformal. The cell resolution footprint on the hull is approximately 0.0022×0.0022 m^2 (1×1 m^2 in full scale). The total number of cells is 3,905,906.

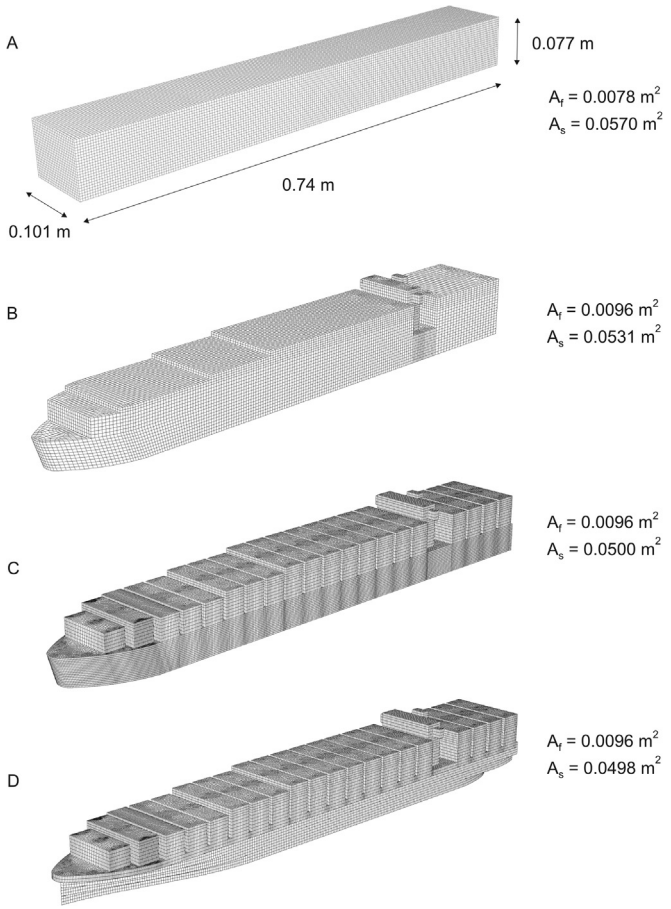

Fig. 6. Computational grid on the surface of four geometrical configurations of the container ship ranging from a simple box (A) to a fairly detailed ship representation (D). Per configuration the projected front (A_f) and side area (A_s) of the ship is given.

Fig. 7 shows the grid on the bottom of the domain for configuration D. Near the ship cell sizes are smaller while further away they gradually increase in size.

4.2. Boundary conditions

For mean wind velocity U (in m/s) the target vertical profile specified by Andersen (2013) and already described in Section 3.2 is used (see Fig. 4).

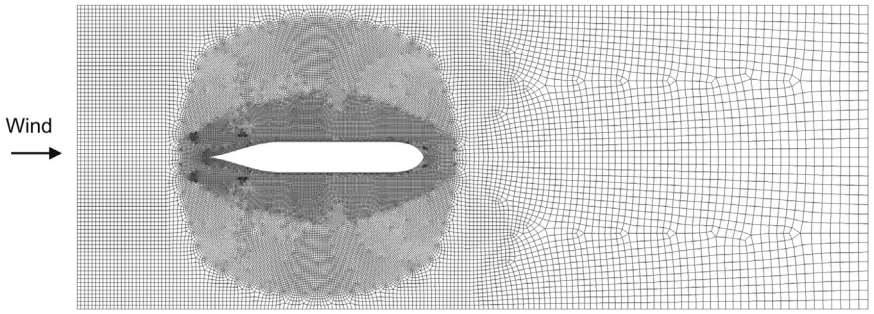

Fig. 7. Computational grid on the ground plane for configuration D.

$$U(z) = U_{ref}\left(\frac{z}{z_{ref}}\right)^{\alpha} \quad (3)$$

with z_{ref}=0.0222 m (equal to 10 m height in full scale), U_{ref}=45 m/s and α=0.11. The vertical profile of turbulent kinetic energy k over height z (Fig. 8a) is based on the target mean velocity profile and the measured turbulence intensity above the turntable:

$$k(z) = I_U(z)^2 \cdot U(z)^2 \quad (4)$$

I_U and U are not measured above 0.1 m; the value for k is therefore assumed constant from 0.1 until 0.7 m height.
The turbulence dissipation rate ε (m^2/s^3), see Fig. 8b, is calculated as:

$$\varepsilon(z) = \frac{u^{*3}}{\kappa(z + z_0)} \quad (5)$$

where κ is the von Karman constant (κ=0.42) and u* the friction velocity calculated by:

$$u^* = \frac{\kappa \cdot U_{ref}}{\ln\left(\frac{z_{ref} + z_0}{z_0}\right)} \quad (6)$$

The actual floor roughness of the wind tunnel is not provided. Therefore, for the CFD simulations, the aerodynamic roughness length for the ground plane of the domain representing water is derived from the updated Davenport roughness classification (Wieringa, 1992): z_0=0.0002 m. At model scale, this yields z_0=4.44*10^{-7} m. The wall function inputs are the parameters k_S (equivalent sand-grain roughness height) and C_S (roughness constant). These parameters are determined from the local values of z_0. The relationship between z_0 and the parameters k_S and C_S was derived by Blocken et al. (2007a, 2007b). For Fluent 6.3, this relationship is k_S=9.793z_0/C_S. This results in an equivalent sand-grain roughness height k_S=4.35*10^{-6} m for a roughness constant C_S =1.

4.3. CFD solution settings

The 3D steady Reynolds-Averaged Navier-Stokes (RANS) equations are solved with the commercial CFD code Ansys Fluent 15 using the control volume method (Ansys, 2013). The realizable k-ε model is used to provide closure (Shih et al., 1995). Second-order discretization schemes are used for both the convective and viscous terms of the governing equations. The SIMPLE algorithm is used for pressure-velocity coupling and standard pressure interpolation is used. Convergence is assumed to be obtained when all the scaled residuals have leveled off. Simulations of the box in the wind tunnel domain with wind angle 10° and 170° did not level off smoothly but showed oscillations with the required second-order discretization schemes, which is at least partly attributed to the fact that the narrow domain influences the average flow results. Regardless, the results of these wind directions remain in line with results of neighboring wind angles and are discussed in Section 6.

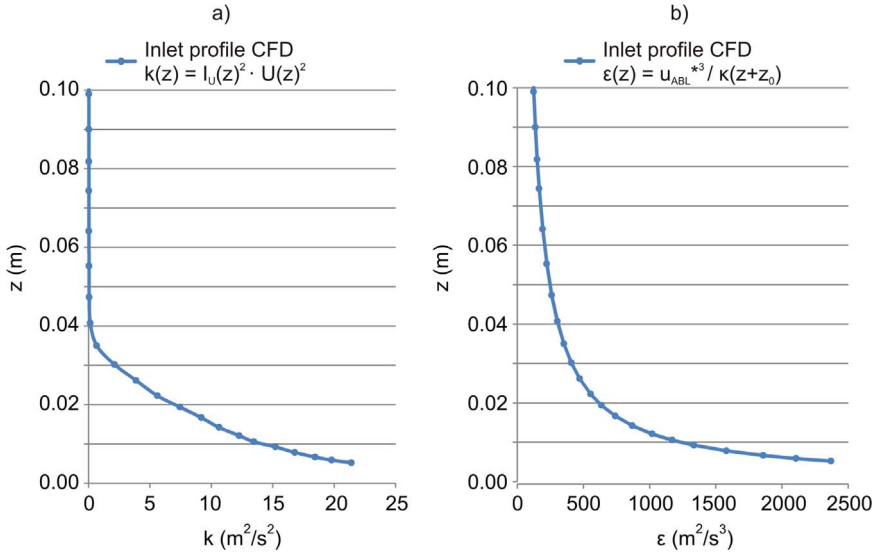

Fig. 8. CFD inlet profiles for (a) turbulent kinetic energy k and (b) turbulence dissipation rate ε.

5. Correction for wind tunnel blockage

For perpendicular approach flow (see Fig. 9), the blockage ratio ($BR=A_{ship}/A_{wind\ tunnel}$) is highest. It ranges from ($0.0498\ m^2/0.70\ m^2$) =7.1% for ship configuration D to ($0.0570\ m^2/0.70\ m^2$)=8.1% for ship configuration A (box). For the measurement setup with a wind tunnel with chamfered corners, a blockage ratio of 7.4% is reported. International Best Practice Guidelines suggest a maximal blockage ratio of 5% for wind tunnel research and 3% for CFD research (Franke et al., 2007; Tominaga et al., 2008) and a directional blockage ratio below 17% (Blocken, 2015). The horizontal directional blockage ratio for perpendicular approach flow is (0.74 m/1.00 m)=74%. Since these guidelines are not fulfilled here, both measurement and simulation results are corrected for blockage.

The CFD results are corrected for blockage in the same manner as done for the experiments by Andersen, following the approach of the Engineering Sciences Data Unit (1980):

$$C_c = C_s \cdot \left(1 - \frac{m \cdot S}{A}\right) \tag{7}$$

where C_c is the corrected coefficient, C_s is the simulated coefficient, m is an expansion factor for the wake (here 3.83, see Andersen (2013), A is the cross-section of the wind tunnel ($0.7\ m^2$) and S is the projected area perpendicular to the flow direction, which is $S_x = A_f \cdot |\cos(\phi)|$ and $S_y = A_s \cdot |\sin(\phi)|$, where ϕ is the wind angle on the ship, as defined in Fig. 5b and A_f and A_s are the projected front and side area of the ship, respectively (see Fig. 6). For the moment, $S_v = A_f \cdot |\cos(\phi)| + A_s \cdot |\sin(\phi)|$ is used. For forces on the front side of the ship the correction is small while for the lateral side the corrections are larger. The blockage ratio, and therefore also the correction factor $(1 - \frac{m \cdot S}{A})$, is largest at wind angles around 90°, as shown in Table 1. The values in Table 1 are for ship configuration D. Similar correction factors are used for the other configurations, following the values for the projected front and side area A_f and A_s of the ship.

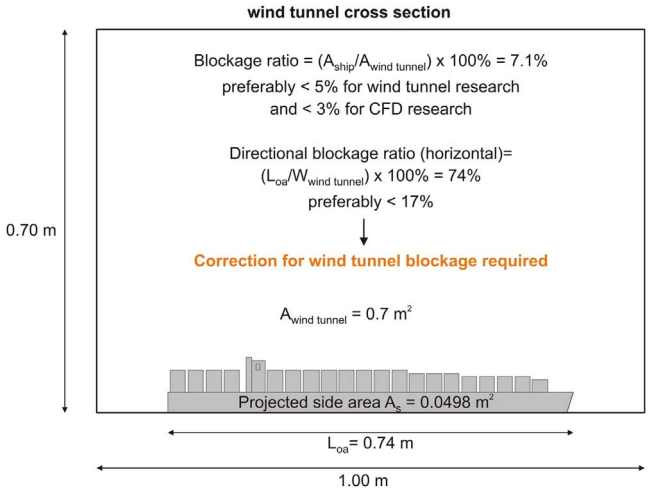

Fig. 9. Blockage ratio and directional blockage ratio for perpendicular approach flow, values for ship configuration D.

6. Results

6.1. Validation

Fig. 10 shows force coefficients C_X, C_Y and the moment coefficient C_N as a function of the wind angle φ ranging from 0° to 180°. Note that the value for C_Y will have a larger effect than C_X on the total wind load on the ship since the projected side area is approximately 5.5 times larger than the projected front area. Overall the detailed configuration D shows the closest resemblance to the wind tunnel data. While configuration C shows the best agreement with the measurements for wind angles 100° (side wind) to 180°, large to very large deviations are found for wind angles 50–70°, both for C_X and C_Y. The least detailed configurations box shape A and configuration B show the overall largest deviations with the experimental data. For example, the average absolute deviation over all 19 wind angles for configuration B is 0.39 for C_X and 0.17 for C_Y, while for configuration D these values are smaller; 0.17 (C_X) and 0.03 (C_Y). Configuration D (slender hull) shows a better agreement with the measurements than configuration C (blunt hull) for wind angles 30° to 90°, showing the importance of modeling the ship bow geometry correctly. Modeling the rear more precisely does not improve the results. For C_N (Fig. 10c), the measured values are generally lower (in absolute values) than the simulated ones and the results for configuration D (detailed geometry) are closest to the measurements. The average absolute deviation over all 19 wind angles for configuration D compared to the experimental data is only 0.006.

For all ship configurations, and all wind angles, the total load is calculated, using the corrected data for wind blockage from Fig. 10 ($F_{total} = \sqrt{X^2 + Y^2}$). Table 2 lists the percentage difference between numerically simulated and measured total wind load on the ship for all ship configurations and all wind angles, as well as the average deviation and the average of the absolute values of the deviations. Averaged over all wind angles, all simulated ship configurations overestimate the wind load on the ship compared to the wind tunnel tests; from an average wind load overestimation of 5.9% for detailed configuration D over 6.9% for configuration C and 17.1% for configuration B to 37.9% for the box configuration A (see Table 2).

Table 1
Correction factors (CF) for blockage in the CFD domain with wind tunnel dimensions for different wind angles on the ship.

φ (°)	0	10	20	30	40	50	60	70	80	90
CF_X	0.947	0.948	0.951	0.955	0.960	0.966	0.974	0.982	0.991	1.000
CF_Y	1.000	0.953	0.907	0.864	0.825	0.791	0.764	0.744	0.732	0.728
CF_N	0.947	0.901	0.857	0.818	0.785	0.758	0.738	0.726	0.723	0.728

φ (°)	100	110	120	130	140	150	160	170	180
CF_X	0.991	0.982	0.974	0.966	0.960	0.955	0.951	0.948	0.947
CF_Y	0.732	0.744	0.764	0.791	0.825	0.864	0.907	0.953	1.000
CF_N	0.723	0.726	0.738	0.758	0.785	0.818	0.857	0.901	0.947

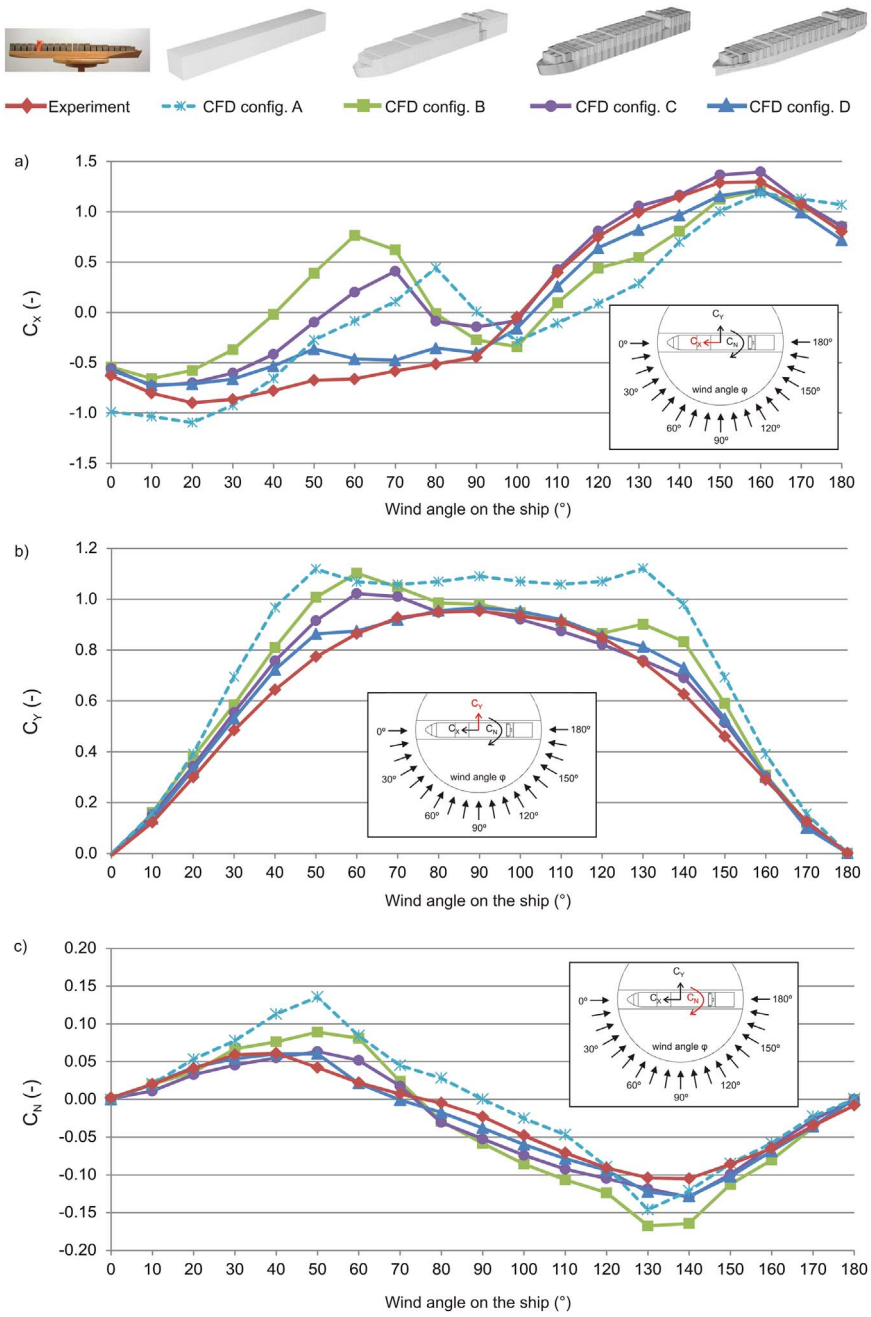

Fig. 10. Comparison of numerical and experimental coefficients as a function of wind angle on the ship for a) the longitudinal force coefficient C_X, b) the lateral force coefficient C_Y, and c) the moment coefficient around the z-axis C_N. Both measured and simulated coefficients are corrected for blockage caused by the wind tunnel geometry.

6.2. *Impact of simplifications of the ship geometry*

The impact of simplifications of the ship geometry is studied with the detailed ship model (configuration D) as a reference. Table 3 lists the percentage deviations of the total wind load for configurations A, B, and C from that of reference configuration D. For C, the average absolute simulated wind load is 5.9% higher than the wind load on ship configuration D which has a more aerodynamically shaped bow. Deviations for configurations B and A are much larger, with on average 14.3% higher wind load on ship configuration B and on average 36.7% higher wind load on the box (A), as compared with configuration D. The difference between ship configuration B and C are the openings between the containers. On average the wind load on ship configuration B is 10.4% (average of absolute percentages) larger than on ship configuration C with the openings, with the largest differences for wind angles 50° and 60°, 130°, 140° and 150°. An even stronger simplification of a container ship than configuration B is the box geometry A. On average over all wind angles the wind load on the box is 20.6% higher than on configuration B.

Table 2
Percentage difference in measured and simulated wind load (F_{total}).

Wind angle (°)	**Percentage difference in wind load with experimental data of** Andersen (2013) $\frac{F_{total,CFD} - F_{total,EXP}}{F_{total,EXP}} \cdot 100\ \%$			
	A 	**B** 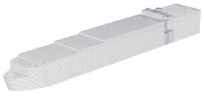	**C** 	**D** 
0	27.5%	−13.0%	−11.4%	−8.6%
10	22.5%	7.9%	4.9%	−1.5%
20	38.5%	21.0%	6.5%	3.0%
30	57.4%	22.2%	10.6%	6.1%
40	67.8%	30.2%	15.3%	10.1%
50	62.8%	36.8%	16.8%	10.1%
60	39.5%	35.1%	17.1%	0.3%
70	29.2%	19.8%	8.5%	−1.5%
80	27.9%	9.7%	−0.6%	0.0%
90	29.9%	8.9%	0.0%	1.0%
100	30.6%	7.9%	−1.4%	1.6%
110	32.0%	5.5%	−4.0%	0.3%
120	41.6%	7.2%	−3.1%	0.1%
130	64.6%	23.9%	0.7%	6.0%
140	69.1%	35.0%	8.6%	12.6%
150	53.6%	25.7%	8.7%	8.3%
160	25.0%	2.0%	1.9%	−3.9%
170	−0.5%	−7.8%	−7.8%	−17.8%
180	−0.5%	−4.5%	−4.0%	−19.2%
Average	**37.8%**	**14.4%**	**3.6%**	**0.4%**
Average abs.	**37.9%**	**17.1%**	**6.9%**	**5.9%**

Table 3
Percentage difference in simulated wind loads of different ship configurations. Configuration D is the reference configuration.

Wind angle (°)	**Percentage difference in wind load with ship configuration D** $\frac{F_{total,CFD} - F_{total,D}}{F_{total,D}} \cdot 100\ \%$		
	A 	**B** 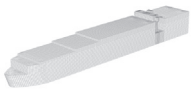	**C** 
0	39.6%	−4.8%	−3.0%
10	24.3%	9.5%	6.5%
20	34.4%	17.5%	3.4%
30	48.3%	15.1%	4.2%
40	52.4%	18.2%	4.7%
50	47.9%	24.3%	6.1%
60	39.1%	34.7%	16.8%
70	31.1%	21.6%	10.2%
80	28.0%	9.7%	−0.6%
90	28.7%	7.9%	−0.9%
100	28.6%	6.2%	−2.9%
110	31.5%	5.1%	−4.3%
120	41.4%	7.0%	−3.2%
130	55.3%	16.9%	−5.0%
140	50.2%	19.9%	−3.5%
150	41.8%	16.1%	0.4%
160	30.0%	6.1%	6.0%
170	21.2%	12.2%	12.2%
180	23.1%	18.2%	18.9%
Average	**36.7%**	**13.8%**	**3.5%**
Absolute average	**36.7%**	**14.3%**	**5.9%**

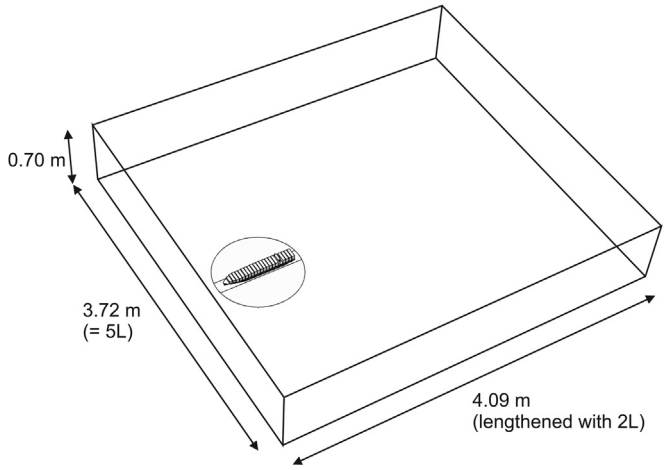

Fig. 11. Larger computational domain with dimensions.

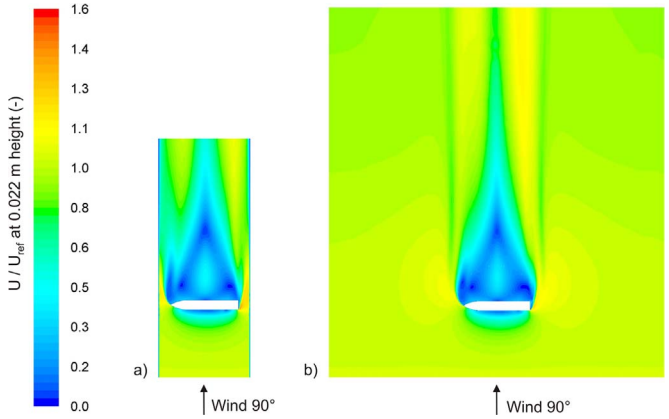

Fig. 13. Contours of normalized wind speed in (a) the wind tunnel domain and (b) a larger domain.

6.3. Larger domain

In CFD it is easy to make a larger domain where the influence of blockage is strongly reduced. For this study the detailed ship configuration D is placed in a larger domain, shown in Fig. 11. At the sides of the domain, symmetry boundary conditions are imposed (i.e. zero normal velocity). Other boundary conditions, and the CFD solution parameters are kept the same.

Fig. 12 shows the results for the lateral force coefficient on the side area of the detailed ship. The solid blue line represents the CFD results corrected for blockage of the wind tunnel, which are very close to the corrected measurement results. The dashed blue line shows the uncorrected force coefficients, while the black line shows these coefficients when the ship is placed in a large domain where blockage is assumed not to interfere with results. Ideally the corrected blue line should overlap the black line, which however is not the case. For a wind angle of 90° the blockage correction following the approach of the Engineering Sciences Data Unit (ESDU) results in an underestimation of the lateral wind load of 17.5%. This implies that the correction factor that is applied for both measurements and numerical simulations is too large. This is substantiated by the fact that the flow field around the ship is quite similar for the wind tunnel and the large domain, particularly in the ship's vicinity, such as the corner streams (see Fig. 13). A potential reason for this deficient blockage correction can be the combination of the large aspect ratio of the ship and the proportionally much lower aspect ratio of the cross-section of the wind tunnel and the computational domain. This combination yields a very large directional blockage ratio (74%, see Section 5) in the horizontal direction and a much smaller one in the vertical direction. The ESDU blockage correction might be more appropriate for lower aspect ratio bodies and/or directional blockage ratios that are less different in horizontal and vertical direction.

7. Discussion

7.1. Velocity inlet profile

Andersen shows that the profile of mean wind velocity gradually changes in the empty wind tunnel test section while ideally this should

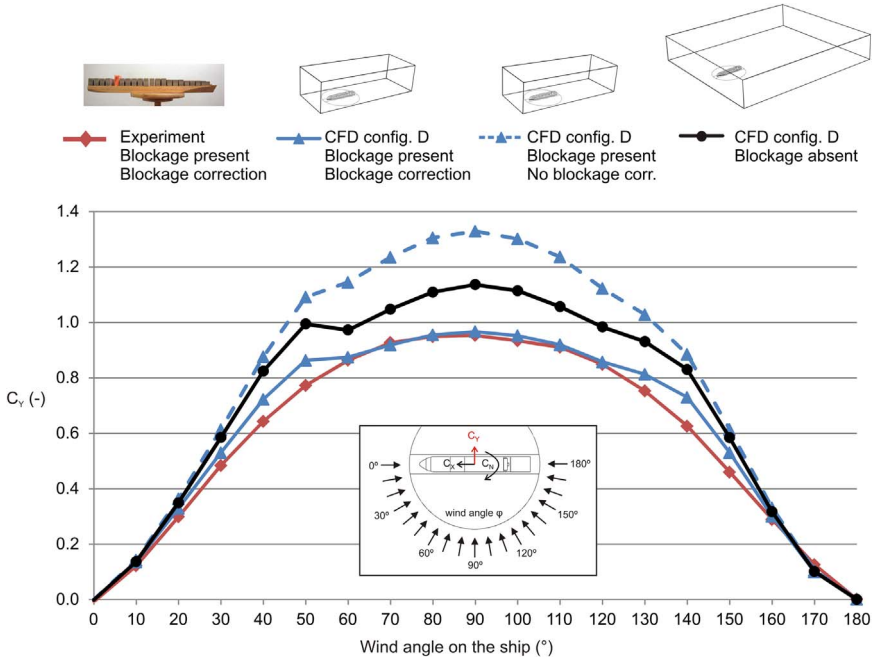

Fig. 12. Comparison between lateral force coefficient corrected (solid red and blue line) and CFD lateral force coefficient not corrected (dotted blue line) for blockage. The black line shows the CFD results for a large computational domain where blockage is not an issue. (For interpretation of the references to color in this figure legend, the reader is referred to the web version of this article.)

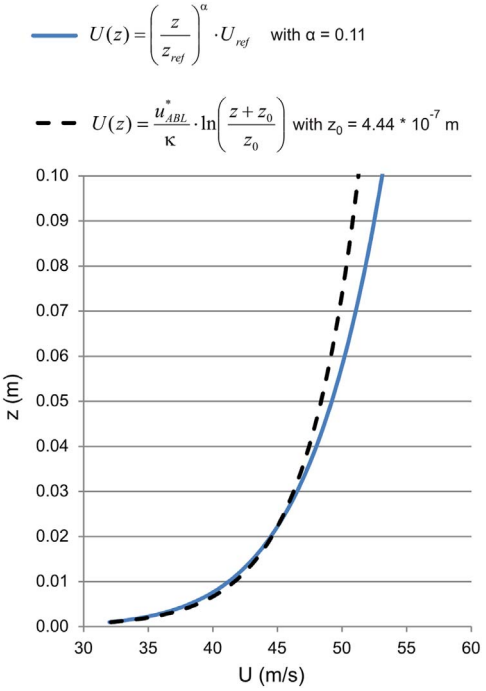

Fig. 14. Target inlet profile (blue) compared to a logarithmic velocity profile (dashed black line). (For interpretation of the references to color in this figure legend, the reader is referred to the web version of this article.)

remain the same. For CFD the choice was made to use the target inlet profile as specified by Andersen. Although the target and measured profiles are rather similar this will affect the comparison of simulated and measured results. The target inlet profile is a power law velocity profile. Instead, a logarithmic velocity profile can be applied:

$U(z) = \frac{u^*_{ABL}}{\kappa} \cdot \ln\left(\frac{z+z_0}{z_0}\right)$,

where u_{ABL}^* is the ABL friction velocity, κ is the von Karman constant and z_0 is the aerodynamic roughness length for the ground plane of the domain representing water (z_0 =4.44*10^{-7} m) as described in Section 4.2. The logarithmic velocity profile is the most often used profile in both experimental and computational wind engineering. Fig. 14 shows the target power law velocity profile (blue solid line) and the logarithmic velocity profile (black dashed line) over the first 0.10 m height of the domain, when matched at z=0.022 m. Below 0.03 m both profiles match closely, above 0.03 m the profiles diverge.

7.2. Blockage effect

The maximum lateral blockage of the wind tunnel is shown to be very high, namely 74%. Therefore both simulations and measurements are corrected for blockage following the approach of the Engineering Sciences Data Unit (1980). However when comparing simulated lateral force coefficients (C_Y) in a larger domain with those in the smaller domain, this correction is shown to be too strong. For wind angle 90° the corrected value of C_Y is 17.5% lower than C_Y in the broad domain. This example shows that obtaining force coefficients from a larger domain should be preferred over correcting for blockage.

7.3. Future work

This paper is a first step towards simulating static wind loads on a berthed container ship in the port to obtain berth requirements such as safe working loads on bollards which is part of the ports infrastructure. However the heterogeneity of the port terrain compared to the homogeneity of the open sea will lead to different force coefficients. The next step is to place container ships in the Port of Rotterdam computational domain and analyze local effects. The results will be described in a future publication.

8. Conclusions

The following main conclusions are drawn:

- Simplifications of the geometry of a container ship can result in very different simulated wind loads on the ship, even though the projected ship areas perpendicular to the wind direction are similar.
- A close agreement was obtained between the CFD simulations of a fairly detailed container ship (configuration D) and the corresponding wind tunnel measurements, with an absolute average difference of simulated and measured wind load on the ship of about 5.9%. Larger deviations were found for the configurations with more simplified geometry: 37.9% for configuration A (rectangular box), 17.1% for configuration B (simple ship geometry with blunt hull, without space in-between container stacks), and 6.9% for configuration C (blunt hull, but with spaces in-between container stacks).
- Modeling the spaces in-between container stacks (configuration C versus B) decreases the average total wind load on the ship. The average of absolute difference for total wind load is 10.4%.
- Modeling the slender ship hull (configuration D) instead of the blunt ship hull (configuration C) decreases the average total wind load on the ship. The average of absolute difference for total wind load is 5.9%.
- Taking into account wind tunnel blockage following the approach of the Engineering Sciences Data Unit showed an underestimation of up to 17.5% for the lateral wind load Y, as evidenced by comparing the CFD results in the narrow domain with those in the wider domain.
- This study shows the importance of validating CFD simulations with measurements. However not many wind tunnel studies of wind loads on container ships are available in the literature. This study also shows that care should be exercised when applying simplified equations for blockage corrections.

Acknowledgement

The authors would like to thank I.M. Andersen for sharing the values of force and moment coefficients (C_X, C_Y, C_N) obtained with the wind tunnel study and the drawings of the wooden ship model. The authors also gratefully acknowledge the partnership with ANSYS CFD.

References

Andersen, I.M.V., 2013. Wind Loads on post-panamax container ship. Ocean Eng. 58, 115–134.
ANSYS Fluent, 2013. Release 15.0. Theory Guide. November, Ansys Inc.
Baker, C.J., 2007. Wind engineering – past, present and future. J. Wind Eng. Ind. Aerodyn. 95 (9–11), 843–870.
Blendermann, W., 1996. Wind Loading of Ships – Collected Data from Windtunnel Tests in Uniform Flow. Bericht Nr. 574. Institut für Schiffbau der Universität Hamburg.
Blocken, B., 2014. 50 years of computational wind engineering: past, present and future. J. Wind Eng. Ind. Aerodyn. 129, 69–102.
Blocken, B., 2015. Computational fluid dynamics for urban physics: importance, scales, possibilities, limitations and ten tips and tricks towards accurate and reliable simulations. Build. Environ. 91, 219–245.
Blocken, B., Stathopoulos, T., Carmeliet, J., 2007a. CFD simulation of the atmospheric boundary layer: wall function problems. Atmos. Environ. 41 (2), 238–252.
Blocken, B., Carmeliet, J., Stathopoulos, T., 2007b. CFD evaluation of the wind speed conditions in passages between buildings – effect of wall-function roughness modifications on the atmospheric boundary layer flow. J. Wind Eng. Ind. Aerodyn. 95 (9–11), 941–962.
Blocken, B., Stathopoulos, T., Carmeliet, J., 2008. Wind environmental conditions in passages between two long narrow perpendicular buildings. J. Aerosp. Eng. – ASCE 21 (4), 280–287.
Engineering Sciences Data Unit, 1980. 80024: Blockage Corrections for Bluff Bodies in Confined Flows.
Franke, J., Hellsten, A., Schlünzen, H., Carissimo, B., 2007. Best Practice Guideline for the Cfd Simulation of Flows in the Urban Environment. COST Office Brussels, ISBN 3-00-018312-4.

Haddara, M.R., Guedes Soares, C., 1999. Wind loads on marine structures. Mar. Struct. 12, 199–209.
Koop, A., Rossin, B., Guilherme, V., 2012. Predicting wind loads on typical offshore vessels using CFD. In: Proceedings of ASME 31th International Conference on Ocean, Offshore and Arctic Engineering (OMAE2012), Rio de Janeiro, Brazil.
Meroney, R.N., 2016. Ten questions concerning hybrid computational/physical model simulation of wind flow in the built environment. Build. Environ. 96, 12–21.
Meroney, R.N., Derickson, R., 2014. Virtual reality in wind engineering: the windy world within the computer. J. Wind Eng. 11 (2), 11–26.
Murakami, S., 1997. Current status and future trends in computational wind engineering. J. Wind Eng. Ind. Aerodyn. 67–68, 3–34.
Norwegian Maritime Directory, 1997. Regulations for Mobile Offshore Units.
Oil Companies International Marine Forum, 1994. Prediction of Wind and Current Loads on VLCCs. 2nd edition.
Shih, T.H., Liou, W.W., Shabbir, A., Yang, Z., Zhu, J., 1995. A new k-ε eddy viscosity model for high Reynolds number turbulent flows. Comput. Fluids 24, 227–238.
SIGTTO, 2007. Prediction of Wind Loads on Large Liquefied Gas Carriers. Technical report, Society of International Tanker & Terminal Operators, Ltd.
Solari, G., 2007. The International Association for wind engineering (IAWE): progress and prospects. J. Wind Eng. Ind. Aerodyn. 95, 813–842.
Stathopoulos, T., 1997. Computational wind engineering: past achievements and future challenges. J. Wind Eng. Ind. Aerodyn. 67–68, 509–532.
Tominaga, Y., Stathopoulos, T., 2016. Ten questions concerning modeling of near-field pollutant dispersion in the built environment. Build. Environ. 105, 390–402.
Tominaga, Y., Mochida, A., Yoshie, R., Kataoka, H., Nozu, T., Yoshikawa, M., et al., 2008. AIJ guidelines for practical applications of CFD to pedestrian wind environment around buildings. J. Wind Eng. Ind. Aerodyn. 96 (10–11), 1749–1761.
van Hooff, T., Blocken, B., 2010. Coupled urban wind flow and indoor natural ventilation modelling on a high-resolution grid: a case study for the Amsterdam arena stadium. Environ. Model. Softw. 25 (1), 51–65.
Wieringa, J., 1992. Updating the Davenport roughness classification. J. Wind Eng. Ind. Aerodyn. 41–44, 357–368.
Wnęk, A., Guedes Soares, C., 2015. CFD assessment of the wind load on an LNG carrier and floating platform models. Ocean Eng. 97, 30–36.